Thermal behavior of resistive ribbon for single-stylus excitation

by Robert A. Laff
Claus D. Makowka

This paper provides a quantitative description of the heating and cooling behavior of the resistive ribbon used in resistive ribbon thermal transfer printing. Since the focus is upon the ribbon, this description has been facilitated by substituting a single, tapered tungsten stylus as a model for a single printhead element. The experiment used an infrared spot pyrometer to measure ribbon surface temperatures downstream from the stylus while a laminate of ribbon and paper was continuously moved beneath the stylus and subjected to current pulses. Measured cooling rates under steady-state excitation at different ribbon velocities showed a behavior consistent with two simple analytic models which describe heat loss into the stylus during heating and two-dimensional diffusion into a half-plane during cooling. A detailed, time-dependent computer simulation using finite-element methods was used to provide a more detailed description of the process by taking into account the local geometry of the heat input distribution and the layered nature of the ribbon-paper laminate. The resulting three-dimensional temperature distributions are given for the steady-state case.

Introduction

The resistive ribbon thermal transfer printing technology [1–7] studied here was recently introduced for use in IBM typewriters and serial printers. It differs from conventional thermal transfer technology [8, 9] in two major respects. First, the printhead consists of an array of compliant elements which may move up and down somewhat independently of one another as the printhead moves across the page. This scheme permits printing on rougher papers than those which can be used with the rigid printhead of the conventional technology. Second, the printhead elements serve as sources of electrical rather than thermal energy. Current passes from the printhead electrodes through a sliding contact into the ribbon, where heat is generated. Since the heat source is only weakly coupled to the large heat capacity of the printhead, increased temporal resolution may be obtained. Placing the heat source in close proximity to the ink tends to provide improved electrical-to-thermal conversion efficiency.

In this paper our major goal is to quantify the behavior of the heating and cooling processes and of the temperature distributions which are produced within the ribbon. The effects of paper roughness are included insofar as they relate to that goal. A brief description of the processes and the methodology used to study them is contained in the following paragraphs.

The heating behavior is complicated because heat flow within the ribbon is bidirectional rather than unidirectional: Only part of the heat generated within the ribbon heats the ribbon and the ink and eventually flows into the paper; the printhead acts as a heat sink for the remaining fraction. A further complication arises because there are three distinct regions of heat generation within the ribbon: at the sliding contact between the printhead and the top surface of the ribbon, in the bulk of the ribbon, and at a thin interface layer between the bulk of the ribbon and an aluminum (ground return) layer. The fraction of heat generated at each location and the conductive paths to printhead and paper

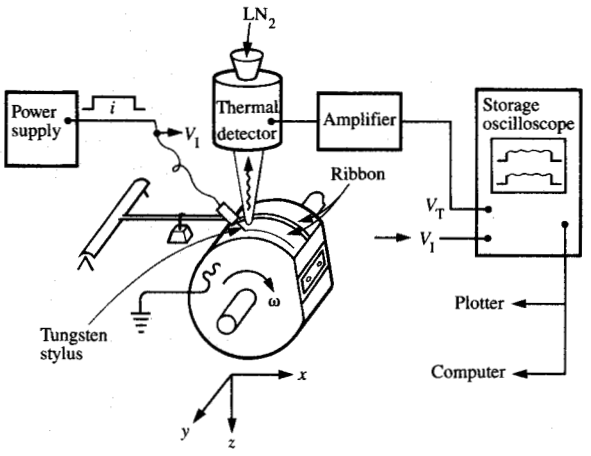

Figure 1

Apparatus for measurement of downstream temperature. The detector is a Barnes Engineering Co. RM-2A radiometric microscope; a Nicolet 4094 digital storage oscilloscope captured the data.

from each source are important factors which determine both the temperature distribution within the ink layer (and thus the characteristics of printing) and the temperature attained by the top surface of the ribbon as it passes beneath the printhead (and thus the fraction of heat lost to the printhead).

The cooling behavior is also important in determining print characteristics, since transfer of the ink to the paper does not occur directly beneath the printhead electrodes, but at a small distance downstream, after the ribbon-ink-paper laminate has emerged from beneath the electrode tips. During the time between heating and transfer the original temperature distribution is broadened by diffusion. The details of the transfer mechanism depend upon the temperature distribution at this later time.

The measurements and most of the analytical methods to be described are for the steady state. We have focused on this mode of excitation in order to obtain a "worst-case" limit for ribbon temperature; this limit is of importance in providing an upper limit to process speed because of ribbon integrity considerations. Even in the steady-state case the heat flow is not easy to analyze, given the multilayer nature of the ribbon-paper laminate and the multiple locations of heat generation. Therefore, we have simplified the system, both analytically and experimentally, by substituting a single stylus for the printhead. This substitution provides a more readily modeled first approximation to the actual printhead and thereby permits us to obtain a tested model of ribbon behavior. It also provides better experimental access to a more local view of the temperature distribution at the free surface of the ribbon, before significant diffusion has occurred. (The geometry of a multielement printhead obstructs the view of the ribbon surface adjacent to the electrode tips, such that radiometric measurements of ribbon surface temperature are restricted to regions in which initially steep thermal gradients have been degraded by diffusion.)

Note: Other related experiments have been performed using a multielement printhead rather than a stylus. In one experiment, the maximum transient temperature of the ink during heating (rather than the downstream temperature of the ribbon surface during cooling) was measured by substituting an infrared transparent substrate for the paper and platen [7, 10]. In another, the printhead temperatures attained during printing were measured [7].

We first describe the apparatus used to measure the quasi-steady-state downstream temperature distribution produced at the free surface of a moving resistive ribbon heated by injection of current through a stationary single electrode. Next, we present steady-state temperature data and discuss briefly the influence of paper roughness on cooling rate. We then analyze the heating and cooling behavior in terms of simple analytic models which ignore both the details of the input heat distribution during heating and the multilayer aspects of the ribbon-paper laminate during cooling. Finally, we further refine the analysis by use of a time-dependent, finite-element computer simulation model which takes into account the laminate structure and treats evolution of heat within the three regions of the ribbon; the relative values of these heat sources, as well as the geometry and the thermal conductivities and capacities of the electrode and various ribbon layers, are parameters of the model.

Experimental apparatus and results

• *Apparatus*

Figure 1 shows the apparatus used to measure ribbon temperatures. Resistive ribbon was wrapped over a paper substrate which was attached to a rubberized metal drum. Both ends of the ribbon were grounded to the drum in a flattened region not covered by rubber. A variable-speed dc motor drive was used to provide single-turn rotation of the drum, thereby causing several inches of ribbon to pass at constant speed beneath the tip of a tungsten stylus. The stylus was inclined at 45 degrees to the normal by means of an insulated holder which was in turn attached to the end of a counterweighted, jewel-pivoted arm of low rotational inertia. Small weights were added to the arm to attain a calibrated contact force of the order of a few grams. The tip of the conical stylus was truncated by polishing to mate with the curved surface of the drum so as to provide a smooth contact surface to the ribbon. The resulting contact area was comparable to that of a single printhead electrode. Lateral micrometer-stage movement of the drum was used to allow a sequence of parallel tracks to be written on the ribbon.

Periodic pulses of constant current were supplied to the stylus (while the drum was in motion), and the voltage between stylus and ground was recorded using one channel of a digital storage oscilloscope. The pulses were of sufficient duration to achieve quasi-steady-state equilibrium. A second channel simultaneously recorded the output from an infrared spot pyrometer focused on the ribbon surface downstream from the stylus. The radiometer had been calibrated by focusing it on the surface of ribbon placed in intimate contact with the thermocouple of a small hot stage. This "substitution" method eliminated the need for knowledge of the emissivity of the ribbon. The detection aperture of the radiometer is a circular disc of approximately 35-μm diameter, so temperatures (which are an average over the aperture) may be measured in close proximity to the tip of the stylus.

There was no attempt to separate the ink from the ribbon, as would be the case in an actual printer; the ribbon and paper remained in intimate contact throughout the cooling process. When the ink cooled to the temperature of solidification, it bonded the ribbon to the paper over a width corresponding to the width of the temperature distribution at that temperature. Temperature measurements were made along the centerline of the heated track as a function of distance downstream from the stylus tip. Data captured by the digital storage oscilloscope were either plotted or sent to a computer for analysis. Voltages and temperatures were measured over a range of input currents, contact forces, downstream distances, and drum speeds. Papers of several different surface roughnesses were used.

• *Measurement results*

This section is a synopsis of experiments performed to obtain the general characteristics of the heating and cooling processes and to study effects of paper roughness on the resultant temperatures.

Figure 2 shows the input power dependence of the time-averaged, quasi-steady-state surface temperature rise (above room temperature) at a distance of 50 μm after emergence of the ribbon from beneath the stylus. The stylus force was varied over a range commonly used in printing. Over the power range shown, the temperature rise ΔT is seen to be rather insensitive to stylus force and to increase linearly with increasing input power. At somewhat higher power, reciprocity failure occurs and the temperature rise is no longer linear with power. Eventually, the ribbon softens and then melts. In the experiments described below, input flux was limited to values for which temperature rise scales with input power.

Figure 3 shows the influence of paper roughness on downstream cooling. The two papers shown provide a range of smoothness from somewhat smoother to very much rougher than that of Fig. 2. The process speed is the same as in Fig. 2. An intermediate stylus force was used. The current

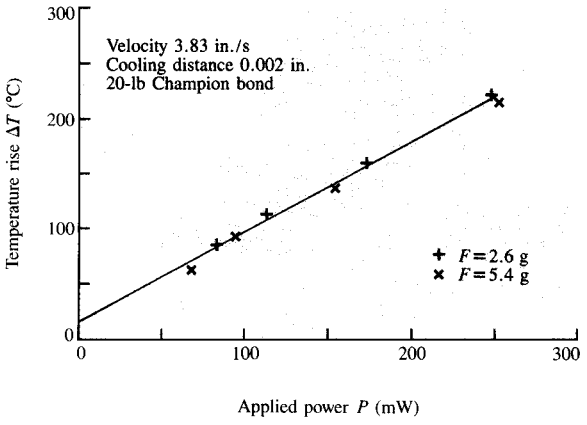

Figure 2

Temperature rise as a function of applied power. Two values of stylus force, above and below normal force range, were used. (Note: 10° offset at zero power is experimental error.)

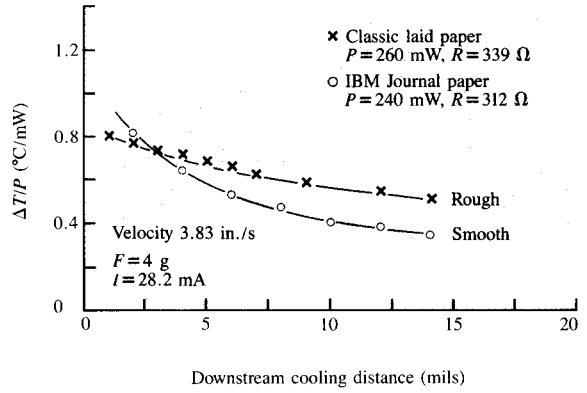

Figure 3

Surface temperature dependence of paper roughness at moderate stylus force. Very rough paper shows lower cooling rate.

was the same for both papers, but, because the total resistance was greater for the rougher paper, the total input power was about 8% greater; the temperatures have been normalized with respect to input power. It is seen that the initial ribbon surface temperature for short times after emergence is somewhat higher for smooth than for rough paper, but that the cooling is more rapid for the former. The data would tend to indicate that paper roughness influences both the net efficiency of ribbon heating and the rate of cooling. (It was also observed that with increasing cooling time the RMS deviations of temperature decayed more rapidly for the smooth paper. Microscopic examination of the interface bond indicated that when very rough paper was used, only local adhesion was obtained between the ink and

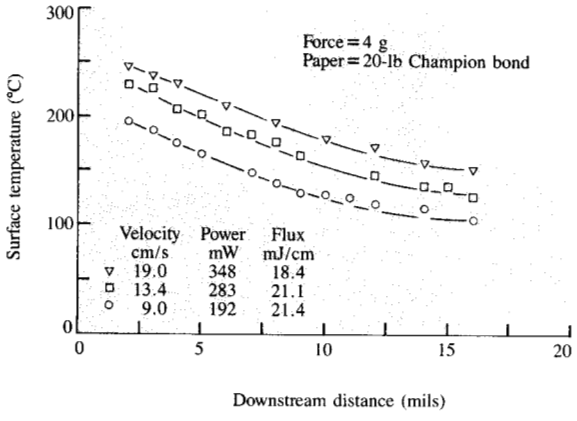

Figure 4

Surface temperature as a function of downstream distance; ribbon velocity as a parameter. Current was adjusted at each velocity to obtain comparable values of flux.

the paper. On the other hand, when extremely smooth plastic films such as ®Mylar [11] or polyimid were substituted for paper, wetting of the ink to the plastic was complete.)

To study the behavior of the sliding contact between the stylus and ribbon, measurements of electrical contact resistance between the stylus and the ribbon were performed using ribbon in which the normally used aluminum layer had been replaced with gold. Gold makes a low-resistance contact to the polycarbonate ribbon material as compared with that obtained for the aluminum, so that a much larger fraction of the total resistance and hence of heat input is localized at the top surface of the ribbon, in close proximity to the stylus. These experiments provided contact resistance data which confirmed that the electrical contact resistance is indeed higher for rougher papers. The data obtained on gold-backed ribbons were also used to analyze input heat distribution within the ribbon, as outlined in the Appendix.

We next investigated the dependence of heating and cooling upon process speed. **Figure 4** shows ribbon surface temperatures obtained for three ribbon velocities, V, as a function of downstream distance. The moderately smooth bond paper of Fig. 2 was used. The input current was adjusted at each velocity in order to produce comparable values of input energy density to the ribbon. At all three velocities the ink was melted during the heating process and a bond was attained between the ribbon and the paper. The cooling curves exhibit a generally similar concave dependence upon distance. These data are analyzed in the following section.

Analysis and discussion of velocity dependence

We begin by providing a simple analytic model for the observed cooling behavior of Fig. 4. Then, heating is treated by two methods of analysis: Initially, we use a very simple analytic method which takes diffusion during heating to be negligible and which ignores both details of initial heat input distribution and the layered nature of the ribbon-ink-paper laminate; later, we use a finite-element simulation in which these considerations are taken into account.

• *A simple analytic model for cooling*

Once the ribbon has emerged from beneath the stylus, the latter no longer acts as a heat sink, so cooling results entirely from diffusion of the heat out through the ribbon and into the paper. For steady-state excitation, the key to solution of the cooling problem is to recognize that in a reference frame which moves with the ribbon, this diffusion is essentially two-dimensional. With the electrode continuously on, to the lowest order of approximation there would tend to be only small temperature gradients in the direction of motion; heat would flow primarily in the lateral (y) and vertical (z) directions with very little cooling due to heat flow in the x-direction. Since diffusivities of the ribbon, ink, and paper are similar (within a factor of three), we have simplified the problem still further by replacing the laminate with a half-plane of average diffusivity a. The problem is then exactly soluble in closed form. Solution of the general cooling problem [12] could be used to provide a surface temperature at the center of the heated stripe after an arbitrary cooling time $t_c = (t - \tau_h)$ in terms of its initial spatial distribution at the termination of heating of duration τ_h, i.e., at $t_c = 0$. Here, for simplicity, we make an additional assumption, as follows: At $t_c = 0$, the net energy per unit length which remains in the half-plane is taken to be distributed within a cross-sectional area having a width comparable to that of the stylus and some small but finite depth. For sufficiently long times $t_c >> \tau_h$, the details of initial heat input distribution become unimportant, and the initially heated cross section can be taken as "thermally thin." Cooling at the surface in the center of the distribution should therefore be similar to that resulting from lateral and vertical diffusion of an initally heated "point" source in two dimensions, i.e., with a temperature which varies inversely with time of cooling. For very short times, the temperature of the source region cannot become arbitrarily large, as would be the case for a source of infinitesimal dimension, but should tend toward a finite limit determined by the specific heat of the initially heated volume. A simple expression which is accurate at both limits, although it may be inaccurate for intermediate times, is

$$T(0, 0, t_c) \approx \frac{T(0, 0, \tau_h)}{1 + t_c/\tau_c}; \qquad \tau_c = A/2\pi a. \tag{1}$$

The quantity τ_c may be taken as a characteristic time for cooling which depends upon both effective diffusivity a and initial distribution. Here, effects of the latter have been absorbed into an effective area

$$A = \frac{1}{T(0, 0, \tau_h)} \int_{z>0} \int T(\tilde{y}, \tilde{z}, \tau_h) d\tilde{y} d\tilde{z}, \quad (2)$$

which represents the cross-sectional area that would have to be heated to a uniform temperature $T(0, 0, \tau_h)$ in order to store the same thermal energy as that stored in the temperature distribution $T(\tilde{y}, \tilde{z}, \tau_h)$. In (1), (2), and hereafter except where otherwise specified, the temperature T refers to temperature rise with respect to room temperature, 21°C.

Figure 5 shows the data of Fig. 4 replotted as the flux-normalized inverse temperature rise P/VT as a function of the cooling time $t_c = X/V$. The straight lines shown are least-square fits to the data. The data for each velocity fall on straight lines, in accordance with the model of Eq. (1), though not on a common curve. First, the characteristic cooling time (i.e., the time increment by which the ordinate increases by a factor of 2 from its value at the $t_c = 0$ intercept) is about 40% longer than the cooling times for the two higher velocities. While the difference might arise from either a smaller value of a or a larger value of A, it is reasonable to suspect the latter. At the lowest speed a larger spread in the initial distribution might be expected, since τ_h (≈0.43 ms) is not negligible with respect to τ_c. Second, the intercepts of Fig. 5 at $t_c = 0$ also exhibit a monotonic increase with decreasing velocity, whereas if losses during heating were small, P/VT should be independent of velocity. This result suggests that losses are velocity-dependent, as would be the case if differing fractions of the total input flux were conducted away by the stylus during the heating period. We now turn to a simple analysis which has the desired behavior.

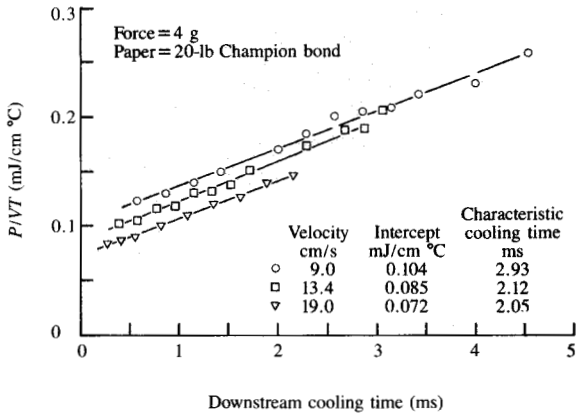

Figure 5

Normalized inverse temperature rise vs. cooling time; ribbon velocity as a parameter. (Note: Both cooling rate and initial temperature are functions of ribbon velocity.)

• *Energy balance analytic model for heating*

We make the assumption that during the heating period the local, instantaneous loss rate to the stylus is proportional to the instantaneous local temperature rise T of the ribbon with a constant of proportionality h, so that the local loss rate is given by hT. When ρC_p is taken as an average heat capacity per unit volume for the polycarbonate, ink, and paper and δ as the depth of the heated area, and the energy flux ϕ is assumed to be uniform and constant during the heating, calorimetric energy balance requires that, at any instant in time,

$$(\rho C_p \delta)(dT/dt) = \phi - hT. \quad (3)$$

This linear first-order differential equation may be integrated over time to get the temperature rise at any time t before emergence:

$$T(t) = \frac{\phi}{h} [1 - \exp -(h/\rho C_p \delta)t]. \quad (4)$$

Since the source is nearly circular, transit time decreases with distance away from the central axis, becoming zero at a distance equal to the stylus radius. However, in the spirit of the approximations already made, we make all transit times equal by substituting for the actual contact a rectangular one which has both the same area, $A_c = \pi D^2/4$, and the same average transit time, i.e, having width D and length in the direction of travel $L = \pi D/4$. Letting $P = \phi A_c$ and $H = hA_c$, and identifying $D\delta$ as A of Eq. (2), at $t = \tau_h = L/V$, we get

$$\frac{P}{VT(V)} = \frac{H/V}{1 - \exp -H/V(\rho C_p A)}. \quad (5)$$

This relationship has all the required properties. For very high velocities V, the argument of the exponent becomes small and we get the adiabatic limit, while for very low velocities, it becomes large and we get the isothermal limit. The experimental results could be compared to the theory if we knew the values of H, A, and ρC_p. We can, however, make a best fit to the data extrapolation for $\tau_c = 0$ by assuming both H and $\rho C_p A$ to be constant. A best fit for the three velocities then gives the loss conductance $H = 0.77$ mW/°C, and the heat capacity per unit length for the initial source, $\rho C_p A = 0.049$ mJ/cm °C.

The average fractions of power retained in the half-space and lost to the stylus may also be calculated by returning to (4) and time-averaging the instantaneous loss rate $hT(t)$ over the heating period. This yields

$$f_r = (\rho C_p A) \frac{V}{H} [1 - \exp -H/(\rho C_p A)V]; \quad f_s = 1 - f_r. \quad (6)$$

We obtain $f_r = (0.47, 0.58, 0.68)$ and $f_s = (0.53, 0.42, 0.32)$ for the velocities (9.0, 13.4, 19.0) cm/s. Thus, in this approximate model, about 1/2 to 2/3 of the input power is effective in heating the ribbon, depending on velocity. These results seem reasonable. However, contrary to the assumptions used here, the cooling data seem to require a weak velocity dependence for H and $(\rho C_p A)$, and further

Table 1 List of material constants and model parameters used in the lumped element model.

Constant or parameter		*Value*
Polycarbonate thickness		15 μm
Polycarbonate heat capacity		1.566 J/cm^3 °C
Polycarbonate thermal conductivity		0.0031 W/cm °C
Aluminum thickness		0.0744 μm
Aluminum heat capacity		3.876 J/cm^3 °C
Aluminum thermal conductivity		1.094 W/cm °C
Ink thickness		5 μm
Ink heat capacity		1.81 J/cm^3 °C
Ink thermal conductivity		0.0027 W/cm °C
Paper thickness		74 μm
Paper heat capacity		1.354 J/cm^3 °C
Paper thermal conductivity		0.0008 W/cm °C
Tungsten heat capacity		2.620 J/cm^3 °C
Tungsten thermal conductivity		1.70 W/cm °C
Stylus taper angle		14.7°
Length of stylus footprint		55 μm
Width of stylus footprint		55 μm
Fraction of input power delivered at stylus contact	ξ	0.54
Fraction of power delivered to bulk of ribbon		0.20
Fraction of power at polycarbonate-aluminum interface	$0.8 - \xi$	0.26
Fraction of contact power dissipation at ribbon surface	η	0.9

Table 2 Comparison of experimental and calculated ribbon temperatures 0.05 mm downstream from the trailing edge of the electrode. The model values are calculated for $\xi = 0.54$ and $\eta = 0.90$ and are scaled to the experimental input powers. The ambient temperature is 21°C.

Velocity (cm/s)	*Power* (mW)	*Experiment T* (°C)	*Model T* (°C)
9	192	193	231
13.4	283	225	283
19	348	242	291

refinement appears appropriate. This was provided by using a finite-element computer simulation model, which we now describe.

• *Finite-element model of ribbon and stylus*

In this section we outline the use of numerical simulation to calculate directly both the heat loss to the stylus and the effective area, A, in the presence of diffusion during heating. Underlying assumptions and major results are shown here; a number of procedural details are to be found in the Appendix.

Both transient and steady-state calculations were performed using ASTAP [13], a finite-element method. The transient solutions would be appropriate for describing the shape of printed single-pel lines during turnon and turnoff. With respect to the energy distributions in the ribbon, the transient response was found to be very fast, achieving 95% of the steady-state value after less than 1 ms. The time constants of the stylus as a whole were found to be very much longer, but they have minimal effect on the thermal behavior of the tip and the ribbon. Since the ribbon transients are so short, the steady-state results are most appropriate for discussing ribbon, ink, and paper temperatures and energy distributions. They also give the maximum ribbon and stylus temperatures, which are of greatest engineering significance. Therefore only the steady-state calculations are described in detail. Furthermore, we show detailed thermal profile results only for the lowest ribbon velocity, 9 cm/s. The quantitative temperatures do depend on ribbon velocity, but the qualitative shapes of the temperature distribution are very similar for all three velocities modeled.

Input power was taken as a linear independent variable. We assumed the power to be directly proportional to current. The latter was assumed to flow directly downward from a conic-section contact area between the electrode and ribbon to the aluminum ground plane in the ribbon. It was assumed that there may exist a thermal contact resistance between stylus and ribbon, but that all other layers are in intimate thermal contact. The ground plane was taken to be dissipationless. It was further assumed that the dimensions and thermal properties of all materials (shown in **Table 1**) are unchanged by temperature and pressure.

Three significant sources of heat are considered: 1) contact resistance at and proximate to the sliding contact between the electrode and the polycarbonate resist; 2) bulk resistance of the polycarbonate; and 3) a nonlinear resistance between the polycarbonate and the aluminum. Experiments not discussed here show that under printing conditions, the bulk resistance of the polycarbonate accounts for only about 20% of the observed impedance between the electrode and the aluminum ground plane [14]. Thus, we assigned 20% of the input power to this heating source. A reliable estimate of the relative sizes of the power input at the sliding contact and the polycarbonate-aluminum interface was not available. Therefore, this was taken to be a parameter of the model. Specifically, if we take ξ as the fraction of the total power which is dissipated in the contact resistance, $(0.8 - \xi)P$ is the power dissipated at the polycarbonate-aluminum interface. To avoid calculation errors introduced by finite mesh size, care must be used in selecting the precise location of power input to a finite-element model. This necessitates the use of a second parameter, η, which distributes that power within the finite mesh size used. Details of how this was done in the present calculation with an ASTAP mesh are to be found in the Appendix. Values of the parameters are summarized at the bottom of Table 1.

Comparison with experiment at short downstream times

Table 2 presents a comparison between the experimental surface temperatures and those derived from the steady-state

model. *(Note that the temperatures given are the actual temperature, not the rise above ambient.)* The model predicts temperatures that are consistently about 20% higher than experiment at all three velocities. Considering the large number of assumptions made, the agreement is reasonable. It is difficult to assign relative importance to possible sources of error, e.g., errors in the material values of Table 1, the omission of phase transitions (i.e., melting/solidification of the ink) from the model, nonlocal deposition of the input power (T. Chieu has experimental evidence for this [15]), and errors in the experimental measurement of temperature.

Temperature profiles

In order to calculate the effective area A of Eq. (2), the steady-state temperature distribution at emergence from beneath the stylus has been calculated. The three-dimensional temperature distributions shown in **Figures 6** and 7 convey the essence of the results. A good way to understand these plots is to imagine following a thin vertical slice of ribbon, seen in cross section, as it moves underneath the stylus. Although the ribbon is in motion, the temperature profile relative to the stylus tip is invariant in time, or in steady state. In the figures, temperatures are plotted vertically and distances from the top surface of the ribbon horizontally, with time along the axis going into the plane of the paper. The temperatures are for volume elements that are just to one side of the centerline of the stylus. In Fig. 6 we are looking in the direction of increasing time from a point before the slice passes under the stylus. Similarly, in Fig. 7 we are looking in the direction of decreasing time from a point after which the slice passes under the stylus.

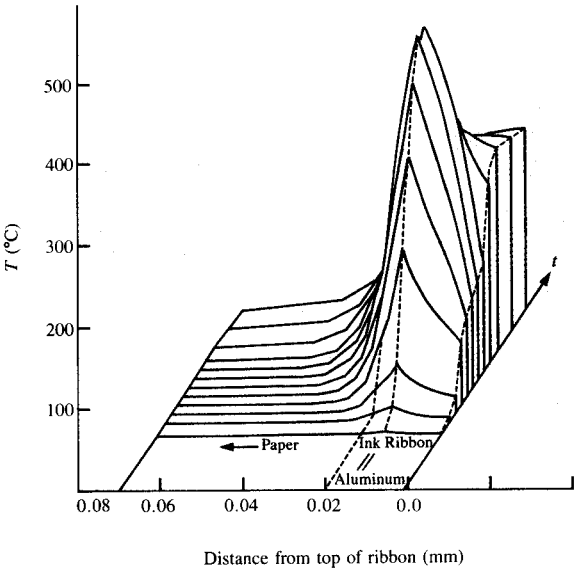

Figure 6

Temperature profiles from the finite-element simulation, showing temperature profile as a function of time and distance from the surface of the ribbon at a place that passes near the center of the stylus. (T in °C is the temperature rise above ambient.) This 3D view looks in the direction of increasing time; later times are farther into the page. Velocity was 3.53 in./s. The time axis is linear: the variable spacing is a result of the variable mesh size used. The smallest separations correspond to time steps of 0.123 ms. Note that the ribbon is much hotter at the interface between ribbon and ink than at the stylus-ribbon contact.

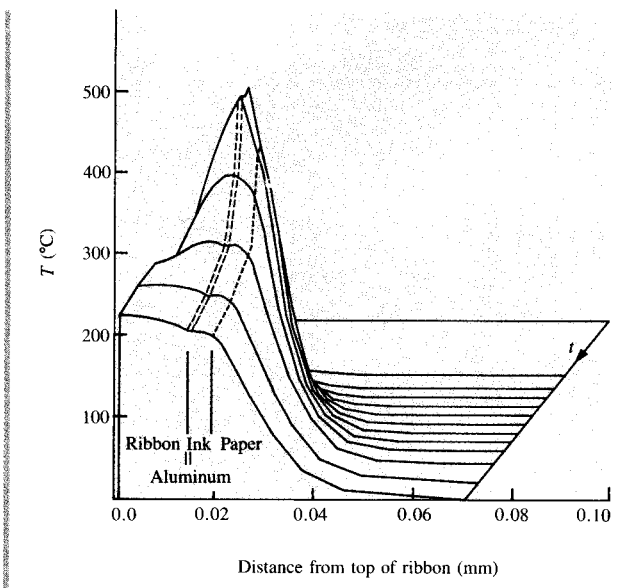

Figure 7

Temperature profiles from the finite-element simulation. Looks in the direction of decreasing time; earlier times are farther into the page. Note the rapid decay of vertical gradients as the ribbon emerges from beneath the stylus. (T in °C is the temperature rise above ambient.)

The most prominent feature is the temperature spike in the center of the figures. This spike, which is at the polycarbonate-aluminum interface, occurs when the ribbon slice is immediately beneath the stylus and is due to the large amounts of power dissipated there. For a power input of 200 mW and a ribbon speed of 9 cm/s, the temperature reaches about 475°C (i.e., the *temperature rise above room temperature* is about 450°C!). Large amounts of power are also dissipated at the top surface of the ribbon, but the model shows that the stylus acts as a heat sink which quickly removes this power, and the temperature of the ribbon surface is only about 145°C. However, upon emergence from beneath the stylus, the free surface of the ribbon rises rapidly, and the ribbon quickly equilibrates to an almost uniform temperature rise throughout its thickness (0.020 mm), being about 250°C at the top and 225°C at the bottom. This is best seen by looking at the front of Fig. 7. There remains a thermal gradient into the paper (which is below

Table 3 Computed values of parameters in single-stylus cooling simulation.

Parameter	*Ribbon velocity V (cm/s)*			*Units of measure*
	9.0	*13.4*	*19.0*	
f_s	0.636	0.606	0.581	
f_r	0.364	0.394	0.419	
A	2.08×10^{-5}	1.80×10^{-5}	1.62×10^{-5}	cm^2
ρC_p	1.60	1.61	1.62	$J/cm^3\,°C$
$\rho C_p A$	0.033	0.029	0.026	mJ/cm °C
H	1.06	1.12	1.19	mW/°C

0.020 mm) and, of course, although it is not shown in the figure, a gradient in both ribbon and paper lateral to the direction of motion. The equilibration time is about 0.5 ms; i.e., at 9 cm/s, equilibration occurs within about 0.05 mm after emergence from beneath the stylus.

Comparison with the energy balance model

All the parameters obtained for the energy balance model can also be computed directly from the finite-element model for each ribbon speed. The total power P_s flowing from the stylus is given directly by the model, immediately giving $f_s = P_s/P$ and f_r. To compute A and ρC_p, a vertical slice perpendicular to the direction of motion is taken immediately following the point where the ribbon emerges from underneath the stylus. We then have A from Eq. (2) using the ribbon surface temperature as $T(0, 0, \tau_h)$. Similarly, we can compute the effective ρC_p by integrating the energy density stored in the slice to give the total stored energy per unit length, which is equated to $\rho C_p A T(0, 0, \tau_h)$. The most difficult parameter to obtain from the finite-element model is H. Since the ribbon surface temperature (which relates most directly to the energy lost to the stylus) is almost constant under the stylus, H is estimated as P_s divided by the average ribbon surface temperature under the stylus. The results are given in **Table 3**.

While the results for the two models are of the same order of magnitude, the specific values are not very close. This arises from slight differences in the assumptions underlying the two models. Recall that the surface temperatures from the experiment and the finite-element model are in reasonably good agreement. Insofar as the analytic model has significantly less power lost to the stylus, the energy density in the ribbon must be higher. Since the ribbon temperatures are the same, this means that the analytic model must have a higher value for ρC_p than the finite-element model. If the differences in f_r are factored out, the models agree to better than 10% for ρC_p. The difference in f_r is a consequence of the different power distributions assumed for the models. The analytic model effectively assumes a uniform power distribution between the ribbon surface and a depth of δ. The finite-element model has a more realistic, very nonuniform distribution of the input power. An estimate compensating for the differing power distributions gives agreement between the models to within 5%. This overall agreement gives us confidence both in our understanding of the experimental data and in the finite-element simulation.

Conclusions

Ribbon cooling behavior is important because in printing the transfer of ink does not occur until some time has elapsed after the period of heating. We have measured and analyzed the cooling of ribbon after it leaves the stylus, for the "worst-case" condition of steady-state excitation. The experimental data can be explained by a simple analytic model for the cooling, via diffusion, of a thin, narrow "point" source on the surface of a homogeneous, two-dimensional half-plane. The cooling rate is a strong function of surface roughness of the underlying paper and a weak function of the process velocity.

Extrapolation of the cooling curves to the time of emergence from beneath the stylus indicates that a significant fraction of the injected power has been lost to the stylus during the heating period. This fraction increases with decreasing ribbon velocity. Using energy balance, we have derived an analytic model for heating. This simple model assumes that heat loss to the stylus is proportional to ribbon temperature rise. It ignores both the local distribution of input power within the system and the presence of diffusion during heating. It was fitted to the data in order to calculate the above constant of proportionality and the fraction of power lost to the stylus.

A detailed numerical simulation of the time-dependent and the steady-state responses to heating has also been made, using a finite-element model. This latter model takes into account the thermal properties of the various layers, and by using a parametric description accounts for a specific local distribution of input power within the ribbon. The parameters are obtained using experiments performed on normal and gold-backed ribbons. A best fit to these experiments requires that about half of the input power be generated at the contact resistance between the stylus and the top of the moving ribbon. The model also predicts a weak dependence on the velocity of the rate at which heat is lost to the stylus. A fit to the data indicates that, depending on ribbon velocity, as much as two thirds of the input power may be lost by thermal conduction to a tungsten stylus. The steady-state simulation was also used to obtain spatial and temporal profiles of the ribbon temperature during transit beneath the stylus and thus to show that the ribbon is much hotter at the the top of the ink layer than at the stylus-ribbon interfacial contact area. This gradient quickly equilibrates within about 0.5 ms after emergence from beneath the stylus.

Simulation of the transient behavior of the stylus-ribbon-paper system after stepwise application of a current shows that although the thermal transient response of the stylus as a whole is slow, the transient response of the stylus tip and of the ribbon is fast. Ribbon temperatures reach about 95% of their steady-state value in about 1 ms.

Appendix

• *Setting up the ASTAP model*

The heat flow problem for the stylus and ribbon is solved in a reference frame fixed to the stylus, with ribbon moving relative to the reference frame. The stylus, ribbon, and paper are divided up into small volume elements with a lumped heat capacity and lumped thermal conductivities to the neighboring volume elements. The volume elements are smaller in regions where temperature gradients are likely to be large, and vice versa. Volume elements within the ribbon-paper layers do not represent fixed pieces of the ribbon or paper; rather, in this region the grid is like a stationary wire frame suspended within a flowing stream of ribbon and paper. Mass transport through the volume elements results in a corresponding energy flow at the velocity of the ribbon in addition to the usual thermal diffusion. Where appropriate, symmetry conditions and thermally insulating boundary conditions are used to minimize computation, by selecting surfaces of the grid to be sufficiently far from the power inputs to ensure negligible heat flow across them. The rubber platen is assumed to be thermally insulating; in practice, the paper is sufficiently thick that little heat gets through the paper and the thermal conductivity of the platen is irrelevant. Although the temperatures on the downstream surface can be high, the temperature gradient is small in the direction of ribbon motion, so there is very little power flowing across this surface due to thermal diffusion. We therefore approximate it as thermally insulating. However, a substantial amount of energy flows out across this surface due to motion of the heated ribbon/paper laminate. This is explicitly accounted for, as is cold ribbon/paper flowing in across the upstream surface.

The stylus is thermally connected to the ribbon at one end and exposed to ambient temperature at the other; it participates as a heat sink as well as a source of current. We note that heat flow in this geometry is isomorphous to that for a hollow sphere heated from the inside, which allows us to calculate the power flowing from the tip of the stylus to the heat sink analytically, as [16]

$$P = \pi r^2 \kappa T_0 \left(\frac{\tan \theta}{r} + \frac{1}{L} \right). \quad \text{(A1)}$$

Here r is the radius of the tip, κ is the thermal conductivity of the tungsten stylus, T_0 is the temperature of the tip, θ is the stylus angle, and the stylus is tied to the ambient $T = 0$ at $x = L$. Obviously, if $L \tan \theta >> r$, the power flowing up the stylus is independent of L for a given tip temperature. This is the case in the model, where we use an L of about 3 cm while $r = 0.00275$ cm and $\tan \theta = 0.129$. A tungsten stylus of this shape thus has a conductance of about 1.9 mW/°C.

• *Heat injection into the ASTAP model*

The ASTAP model represents volume elements by lumped values located at the center of the volume element. Thus, all the power dissipated in a volume element is applied at its center. If the power dissipation is not uniform throughout the volume element, an error is made, which is most serious if the power dissipation is large and the centroid of the power distribution is not at the center of the element. This is an especially important point here because the vertical distribution within both interfaces appears to be over distances that are significantly less than the height of the volume elements used in the model. Computational constraints preclude use of smaller volume elements.

The interface layer between the polycarbonate and the aluminum may be treated in a straightforward manner by selecting the volume element containing it such that the interface runs through the center of the volume element. Then the centroid of the power distribution and the center of the volume element coincide, and there is no computational error. The aluminum layer is centered vertically in the appropriate volume elements.

The dissipation due to the contact resistance between the sliding electrode and the ribbon surface is more difficult to model since the details of the distribution are unknown. We expect the dissipation to occur within the polycarbonate resistive layer; hence, it is unphysical to assume that the power input is precisely at the interface between the electrode volume elements and the topmost ribbon volume elements. On the other hand, distributing it uniformly in the latter evidently overestimates the thermal contact resistance, because the temperatures calculated from the model are then dramatically higher (by almost a factor of 2) than experiment. Because the model is linear, one can interpolate between these extremes by dividing the power between these alternatives. Physically this means that dissipation is occurring somewhere below the interface but above the center of the topmost volume elements. A model parameter η selects the fraction of the contact resistance dissipation which is applied exactly at the interface between the electrode and the ribbon. The remainder is applied in the top layer of volume elements in the ribbon. The final results are not very sensitive to the exact choice of η.

• *Parameters for heat input distribution*

Here we describe selection of values for the parameters ξ and η. Experimental temperatures for aluminum-backed and gold-backed ribbon at a ribbon velocity of 9 cm/s were compared to give an equation relating ξ and η. The value of

η was then selected to give the best agreement between the model and experiment for normal aluminum-backed ribbon at the same velocity.

At any given point, the temperature computed by the model as a function of ξ and η always obeys the relationship

$$T = T_0 + a\xi + b\xi\eta, \tag{A2}$$

where T_0, a, and b are constants depending on the input power and the position. In terms of the model, the difference between aluminum-backed and gold-backed ribbon is the difference in the power distribution implied by ξ. Since there is no high-resistance layer in the gold-backed case, $\xi_{Au} = 0.8$. (Recall that the model assumes that 20% of the power is dissipated in the bulk of the ribbon.) We seek to find ξ_{Al}. If T_{Au} and T_{Al} are the ribbon temperatures of gold- and aluminum-backed ribbons, respectively, for the same input power, then using Eq. (A2) we have

$$\frac{T_{Au}}{T_{Al}} = \frac{T_0 + 0.8a + 0.8b\eta}{T_0 + a\xi_{Al} + b\xi_{Al}\eta}. \tag{A3}$$

Experimentally this ratio is observed to fall between 0.5 and 0.6, from which we selected the value 0.54, for a ribbon velocity of 9 cm/s. Once the parameter η is selected, ξ can be calculated from Eq. (A3). In writing down Eq. (A3) it is assumed that η is the same for both kinds of ribbon. This seems reasonable since the top of the ribbon is physically the same in both cases, except for the temperature. The details of the contact depend on the deformation of the ribbon under the stylus. If this deformation were temperature-dependent, η would be temperature-dependent and different for the two ribbons. In the spirit of the model, however, η is assumed to be temperature-independent, hence the same for both ribbons. There is no obvious temperature-related change in the contact resistance which calls this assumption into question. We chose η by comparing the temperatures from the model as a function of η with the experimental temperature, for a ribbon velocity of 9 cm/s. For $\eta = 1$, the computed temperature was slightly too low, while it was similarly a little too high for $\eta = 0.9$. Given the other approximations in the model, pressing for a more precise value of η was not justified, leading us to use $\eta = 0.9$, with the corresponding value of $\xi = 0.54$.

Acknowledgments

We are deeply indebted to Derek Dove for many stimulating discussions and helpful suggestions throughout the course of this work, and to Eric Lean for continued interest and encouragement. We also appreciate Bob Wooton's assistance in learning about an earlier computer simulation which combines the thermal and electrical behavior. This proved very helpful in the design of the model described here. We would also like to thank Richard John for his valuable assistance in setting up the apparatus and taking the measurements.

References and note

1. L. Montanari and F. Knirsch, "Electro-Thermic Printing Device," U.S. Patent 3,744,611, 1973.
2. J. L. Mitchell and K. S. Pennington, "Thermal Transfer Printer Employing Special Ribbons with a Current Pulse," *IBM Tech. Disclosure Bull.* **18**, No. 8, 2695 (1976).
3. K. S. Pennington and W. Crooks, "Resistive Ribbon Thermal Transfer Printing (R2T2): A New Printing Technology," *Technical Abstracts,* Second International Congress on Non-Impact Printing, Society of Photographic Scientists and Engineers, Springfield, VA, 1984, p. 236.
4. W. Crooks and K. S. Pennington, "Resistive Ribbon Thermal Transfer Printing, Ribbon and Head Requirements," *Technical Abstracts,* Second International Congress on Non-Impact Printing, Society of Photographic Scientists and Engineers, Springfield, VA, 1984, p. 237.
5. W. Crooks, D. M. Shattuck, J. Tsay, W. Weiche, and K. Pennington, "Resistive Ribbon Thermal Transfer Printing," *Technical Abstracts,* Paper 9.3, SID Symposium, Orlando, FL, 1985.
6. R. A. Laff and R. A. John, "Print Fidelity of Resistive Ribbon Thermal Transfer Printing," *Technical Abstracts,* Paper 9.4, SID Symposium, Orlando, FL, 1985.
7. O. Sahni, T. C. Chieu, D. B. Dove, R. A. Laff, R. Lane, and S. I. Tan, "Thermal Characterization of Resistive Ribbon Printing," *Technical Abstracts,* Paper 9.5, SID Symposium, Orlando, FL, 1985.
8. J. L. Yoder and E. Webster, *Thermal Transfer Printing: Technology, Products, Prospects,* L. Mirowitz and F. A. Stefansson, Eds., DATEK Information Services, Inc., Newtonville, MA, 1983.
9. T. Tsuruoka, S. Shibata, K. Otsubo, and K. Nihei, "Printing Characteristics of High Resolution Thin Film Thermal Printing Head," *Technical Abstracts,* Second International Congress on Non-Impact Printing, Society of Photographic Scientists and Engineers, Springfield, VA, 1984, p. 242.
10. T. C. Chieu and O. Sahni, "Ink Temperatures in Resistive Ribbon Thermal Transfer Printing," *IBM J. Res. Develop.* **29**, 509–518 (1985, this issue).
11. ®Mylar is a registered trademark of E. I. du Pont de Nemours and Co., Wilmington, DE.
12. H. S. Carslaw and J. C. Jaeger, *Conduction of Heat in Solids,* 2nd Ed., Clarendon Press, Oxford, England, 1959, pp. 230–231 (see also A. V. Luikov, *Analytical Heat Diffusion Theory,* Academic Press, Inc., New York, 1968, p. 119).
13. IBM Program Product No. 5796-PBH, *Advanced Statistical Analysis Program (ASTAP), Version 10,* Order No. SH20-1118-0, available through IBM branch offices.
14. K. K. Shih, IBM Research Division, Yorktown Heights, NY, private communication.
15. T. Chieu, IBM Research Division, Yorktown Heights, NY, private communication.
16. Carslaw and Jaeger, *op. cit.,* p. 258.

Received October 22, 1984; revised April 24, 1985

Robert A. Laff *IBM Research Division, P.O. Box 218, Yorktown Heights, New York 10598.* Dr. Laff is a Research staff member in the Input-Output Technologies Department at the Thomas J. Watson Research Center. After receiving his training in physics at the California Institute of Technology, University of Illinois, and Purdue University, he joined IBM in 1960. He has worked in several areas of exploratory materials, techniques, devices and device packaging, including transport and optical properties of semiconductors, thin film devices, surface wave acoustics, and laser recrystallization. Since 1977 he has been involved in the study of electrophotographic and thermographic printing. He received an IBM Outstanding Contribution Award for his work in gallium arsenide lasers and is the recipient of three IBM Invention Achievement Awards. He is a member of the American Physical Society, the Institute of Electrical and Electronics Engineers, and the Society for Information Display.

Claus D. Makowka *IBM System Products Division, P.O. Box 1328, Boca Raton, Florida 33432.* Dr. Makowka holds a B.S. in physics from the California Institute of Technology and M.S. and Ph.D. degrees in physics from the University of Illinois at Urbana-Champaign (1982). He joined IBM in 1982, working on studies of resistive ribbon printing at the Research Division in Yorktown Heights. Dr. Makowka is currently developing system microcode in Boca Raton and has received an IBM Outstanding Technical Achievement Award for microcode development for an advanced-function printer.